Available online at www.sciencedirect.com
SCIENCE DIRECT®
Journal of Molecular Catalysis A: Chemical 239 (2005) 116–124
JOURNAL OF MOLECULAR CATALYSIS A: CHEMICAL
www.elsevier.com/locate/molcata

Sulfur adsorption and sulfidation of transition metal carbides as hydrotreating catalysts

Ping Liu, José A. Rodriguez *, James T. Muckerman

Department of Chemistry, Brookhaven National Laboratory, Bldg. 555, Upton, NY 11973, USA

Received 19 April 2005; received in revised form 31 May 2005; accepted 2 June 2005
Available online 18 July 2005

Abstract

The formation of MoS_xC_y compounds has been observed on/in the surface of molybdenum-sulfide catalysts during the hydrodesulfurization (HDS) process, and it is a major factor for determining the activity of molybdenum-carbide catalysts. Density functional theory (DFT) was employed to investigate the adsorption of sulfur and sulfidation of transition metal carbides from groups 4–6 in the periodic table, including extended surfaces [MC(0 0 1) (M = Ti, V, Mo, Ta)], nanocrystals [$M_{14}C_{13}$ (M = Ti, V, Mo)] and metcar [M_8C_{12} (M = Ti, V, Mo)] nanoparticles. It was found that with increasing carbon/metal ratio, the reactivity of the metal carbides towards sulfur decreased in the sequence: $Mo_2C > M_{14}C_{13}$, $M_8C_{12} >$ MC(0 0 1). In terms of sulfidation, M_8C_{12} and MC(0 0 1) display a stronger resistance than $M_{14}C_{13}$. The presence of corner or edge sites in the $M_{14}C_{13}$ nanocrystal favors the formation of MoS_xC_y compounds. Following Sabatier's principle, our results suggest that flat MC(0 0 1) surfaces are too inert to catalyze HDS reactions, while $M_{14}C_{13}$ is too active to resist the sulfidation that leads to degradation of the carbides. For reactions involving sulfur and sulfur-containing molecules, nanoparticles adopting the special geometry of metcars should display a better catalytic activity than the corresponding bulk materials and carbide nanoparticles that have a cubic-based structure like nanocrystals. Indeed, DFT calculations indicate that Ti_8C_{12} and Mo_8C_{12} are good catalysts for the HDS of thiophene.

Keywords: Sulfur adsorption; Sulfidation; Density functional theory; Metal carbide; Nanocrystal; Metcar

1. Introduction

Sulfur-containing molecules are common impurities in oil. The sulfur present in these impurities poisons catalysts used for the conversion of oil-derived feedstocks and produces sulfur oxides (SO_x) during the burning of fuels [1–3]. In the hydrodesulfurization (HDS) process, sulfur-containing molecules are removed from petroleum by reaction with hydrogen to form H_2S and hydrocarbons [2,4]. The industrial HDS catalysts are complex systems [2], and usually consist of a mixture of MoS_2 and Co or Ni on a γ-alumina support [4]. The exact nature of the active sites in these systems is a matter of debate. It has been shown that MoS_xC_y compounds are formed on/in the surface of molybdenum sulfide catalysts during the HDS process [5]. With new environmental regulations stressing the need for a reduction of the content of sulfur in transportation fuels, searching for better HDS catalysts has become a very important issue in catalysis [4,6]. Metal carbides could be useful in this respect [6,7].

The early-transition metal carbides have attracted considerable attention after the discovery in the 1970s that they have catalytic properties similar to those of expensive noble metals [8–10]. Pure early transition metals are elements that are too reactive to be useful as catalysts. The inclusion of C into the lattice of an early transition metal produces a substantial gain in stability [11], while the chemical activity decreases due to a downshift of the metal d-band center (ligand effect) and missing metal sites not available for interactions with adsorbates (ensemble effect) [9–14]. Thus, according to Sabatier's principle [15], metal carbides should be good catalysts [11,12,14]. A series of studies have found that Mo_2C possesses excellent catalytic properties for hydrotreating reactions [2,3,16–18], but its activity decreases

* Corresponding author. Tel.: +1 631 344 2246; fax: +1 631 344 5815.
E-mail address: rodrigez@bnl.gov (J.A. Rodriguez).

1381-1169/$ – see front matter © 2005 Elsevier B.V. All rights reserved.
doi:10.1016/j.molcata.2005.06.002

rapidly with time [7,9,10,17,18]. The degradation of Mo_2C catalysts was ascribed to the formation of a chemisorbed layer of sulfur or MoS_xC_y compounds on the surface of the catalyst [6,7,19]. This phenomenon in general is not well understood and it is not known how it will depend on the properties of the metal centers, the structure of the system, or the carbon/metal (C/M) ratio in a carbide.

In the present study, density functional theory (DFT) [11–14,20–22] is employed to investigate sulfur adsorption and sulfidation of metal carbides including extended surfaces of MC(0 0 1) (M = Ti, V, Mo, Ta), nanocrystals $M_{14}C_{13}$ (M = Ti, V, Mo), as well as metallocarbohedrenes (metcars), M_8C_{12}. Metcars and nanocrystals are well-known components of metal carbides [11,12,23–27]. Interest in these nanoparticles stems from their unusual properties including ionization in gas phase, bonding and reactivity [11,12,23–27]. Although one would expect a decrease in activity when raising the C/M ratio, recent DFT calculations show that metcars (C/M = 1.5) and nanocrystals (C/M = 0.93) are very active towards CO, H_2O, NH_3 and SO_2, while being very robust at the same time [11,12,23]. Furthermore, these nanoparticles seem to exhibit good catalytic activity for the HDS of thiophene [14]. To our best knowledge, no systematic study has been reported for the interaction of sulfur with metal carbide systems. According to the calculated S adsorption energies and the energetics of sulfidation, we can screen the catalysts that possess a moderate bonding strength, being able to resist sulfidation while still being able to break the C-S bonds (Sabatier's principle [15]). Following this idea, our DFT results show that by virtue of their unique structure, the M_8C_{12} nanoparticles should be good catalysts for HDS. In contrast, the MC(0 0 1) surfaces are too inert to catalyze HDS reactions, while the $M_{14}C_{13}$ nanoparticles are too active to resist sulfidation.

2. Theoretical method

Our all-electron DFT calculations were performed using the DMol[3] code, which allows modeling the electronic structure and energetics of molecules, solids, and surfaces [28–31]. A double numerical basis set of accuracy comparable to a Gaussian 6–31 G(d) was employed with a local basis cutoff of 5.5 Å in real space. When a more extended basis set and a higher cutoff were tested, no remarkable changes appeared. The generalized gradient approximation (GGA), with the revised version of the Perdew–Burke–Ernzerhof (RPBE) functional [32], was used in the present work. This functional, highly recommended for chemisorption studies [21,22,32], usually shows absolute errors in adsorption energy of ~0.2 eV [32]. Our main interest here is the *trend* in the energetics, and in test calculations these were not affected when other GGA functionals (Becke–Perdew; Perdew–Wang 91) were used. DFT calculations with both restricted spin and unrestricted spin were tested for the metcars and surfaces, leading to energy differences of less than 0.2 eV. The results described below were obtained with spin-restricted DFT. Other theoretical studies also pointed out the ground states of M_8C_{12} as a closed shell [24,33]. In many of our studies for the metcars, nanocrystals and extended surfaces, we found that the level of theory used in this article reproduced reasonably well experimental data reported for vibrational spectra [24,34–36], surface structures [13], and adsorption energies [11,12,31].

For adsorbed S, several possible sites were considered here. In the calculations, the adsorbates and metcars were allowed to relax in all dimensions. The bulk carbide surfaces were modeled following the supercell approach with four-layer slabs [13,37,38] and a 11 Å vacuum between the slabs (Fig. 1a). The surface Brillouin zone was sampled at 21 or 16 K-points [11–13,23]. The adsorption of S on carbides at coverages of 1/4 and 1/2 of a monolayer (ML) is included for the bulk surfaces, which corresponds to one and two S atoms bonded to a carbide nanoparticle, respectively. Here, we consider that the equilibrium corresponds the enthalpy of reaction for the process, $H_2S_{gas} \rightarrow H_{2,gas} + S_{ads}$. The reverse reaction includes the adsorption of a S atom, and therefore

$$E_S = E\left(\frac{nS}{surf}\right) + nE(H_2) - E(surf) - nE(H_2S) \quad (1)$$

was used to describe the S adsorption energy, where "*n*" is the number of additive S atoms per cell. The more negative the adsorption energy, the more difficult the removal of S in the form of gaseous H_2S. The top three layers of the bulk surfaces were allowed to relax along with the adsorbates, while only the bottom layer was kept fixed at the calculated bulk lattice positions. All the geometries for the surface, nanocrystal and metcar systems were optimized with no symmetry constraints. In addition, for each optimized structure, a Mulliken population analysis [39–42] was carried out to estimate the

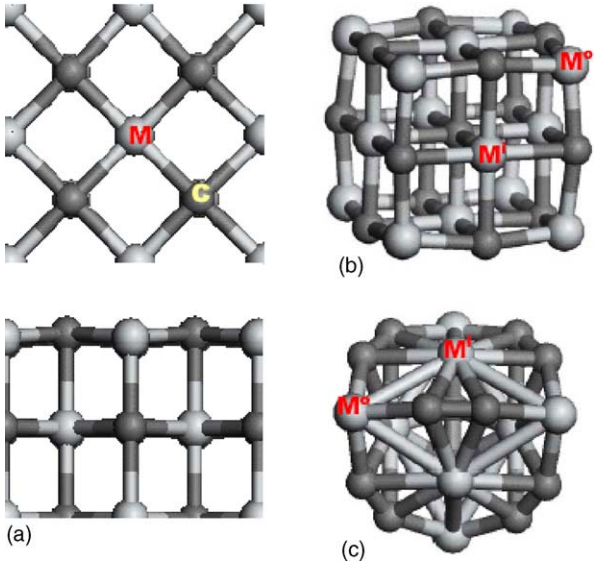

Fig. 1. Optimized configurations of the extended surfaces MC(0 0 1) (upper: the top view; lower: the side view) (a), nanocrystals $M_{14}C_{13}$ (b) and metcars M_8C_{12} with T_d symmetry (c).

partial charge on each atom and examine *qualitative trends* in charge redistribution. When using the Mulliken method, one has to be careful with the type of basis set used [40–42]. The basis set employed here and the Mulliken analysis give charge distributions for Ti_8C_{12} that are close to those obtained with charges derived from fitting electrostatic potentials using grid-based methods (CHELPG) [11,12,24]. In addition, our main interest in this study is the change in the partial charge on each atom with metal/carbon ratio and structural configurations.

3. Results and discussion

This section is organized as follows. First, we will compare the geometries of the different metal carbide systems investigated, followed by examining the energetics for the chemisorption of sulfur and the formation of MoS_xC_y compounds. On this basis, we will try to predict the metal carbide systems that are S-resistant and can perform the catalytic HDS of thiophene well.

3.1. Geometry of metal carbides

The metal carbides in this study include bulk metal monocarbides (MC), nanocrystals ($M_{14}C_{13}$) and metcars (M_8C_{12}). All the bulk MC in which we are interested have a well-known NaCl structure with a fcc Bravais lattice [9,43–46]. The DFT-RPBE calculated lattice constants for TiC, VC, δ-MoC and TaC are 4.34, 4.17, 4.36 and 4.44 Å [11–13,23], respectively. These values are in good agreement with the corresponding experimental measurements (4.33 [44], 4.16 [45], 4.33 [46], and 4.46 Å [47]). For the MC(0 0 1) surfaces, our calculations as well as other studies show that there is a considerable zigzag in the surface with the surface C atoms moving slightly outwards and the M atoms inwards (Fig. 1a) [10,46]. This phenomenon is studied in detail in Refs. [11,13,47].

The $M_{14}C_{13}$ nanocrystal is a $3 \times 3 \times 3$ cube (Fig. 1b) with C in the center and at the midpoints of each of the twelve edges, plus M atoms at the eight corners (M^o, Fig. 1b) and six face midpoints (M^i, Fig. 1b). $Ti_{14}C_{13}$ and $V_{14}C_{13}$ were experimentally observed as a completely fcc fragment of bulk TiC and VC, respectively [25,26,34]. $Mo_{14}C_{13}$ has never been observed experimentally but was constructed theoretically as the fcc fragment of bulk δ-MoC for comparison. Our calculations show that the $M_{14}C_{13}$ species adopt a configuration with M^o drawn inwards slightly after the optimization (Fig. 1b) [23]. Such a configuration leads to a vibrational spectrum in excellent agreement with that measured experimentally for $Ti_{14}C_{13}$ [23,25]. In addition, we also consider $M_{14}C_{13}$ as the analog of the step edges and kinks present in non-ideal MC(0 0 1) surfaces. Although the size of the nanocrystal is much smaller, the chemical activities are dominated by the atoms with lower coordination in both systems and should be similar.

All the M_8C_{12} nanoparticles prefer a T_d or slightly distorted T_d-like structures (D_{2d} and C_1) [11,12,14,23,24,33] rather than a dodecahedral T_h structure [26,27] by about 10eV. The calculated vibrational spectra using the T_d-like structures were in accord with the experimental observations [23,25]. The T_d structure for M_8C_{12} is based on a M_8 tetracapped tetrahedron (Fig. 1c). Eight metal atoms occupy two different positions: four low-coordination outer atoms (M^o), and four high-coordination inner atoms (M^i). T_d-like structures (D_{2d} and C_1) were constructed by slightly perturbing some of the bond lengths to decrease the symmetry. A T_d-like structure with C_1 symmetry was considered here.

3.2. Sulfur adsorption on metal carbides

Sulfur adsorption is of fundamental importance in many catalytic systems [48]. A number of theoretical studies of sulfur adsorption on metal surfaces have been reported [24,49,50]. However, little has been done for the metal carbides [11–13], although they seem very active for the dissociation of sulfur-containing molecules [9,16,51]. It is usually assumed that the C atoms in metal carbides are simple spectators in hydrotreating reactions [5,9,51]. Previously, we have examined the adsorption of S on some metal–carbide systems [11–13]. Here, we will present a more systematic study.

For MC(0 0 1) surfaces, S adsorption was considered above M atop (T) sites, M–M bridge (B) sites, hybrid M–C bridge (HB) sites and hybrid hollow (HH) sites constructed by two metal atoms and one C atom (M–C–M) (Fig. 2a). Table 1 lists the calculated S adsorption energies at a coverage of 1/4 ML. The most favorable site for S adsorption on all the MC(0 0 1) surfaces is the HH site. S atoms at the HB sites either spontaneously shift to the HH sites of MC(0 0 1), or weakly bond with these carbide surfaces. As we will see below, the metal centers in MC are greatly deactivated due to a large electron transfer to the C neighbors, which leads to a chemical activity comparable to that of the C atoms. Thus, *the C atoms of MC*(0 0 1) *surfaces play a direct role in the*

Table 1
Calculated S adsorption energy on metal carbide surfaces, nanocrystals and metcars at low S coverage (1/4 ML), E_S (eV)

	TiC(0 0 1)	VC(0 0 1)	δ-MoC(0 0 1)	TaC(0 0 1)
HH	−0.85	−0.20	−0.78	−0.43
HB	0.12	⇒ HH	−0.12	−0.01
T	⇒ HH	⇒ HH	0.27	−0.37
	$Ti_{14}C_{13}$	$V_{14}C_{13}$	$Mo_{14}C_{13}$	
HH	−1.58	−1.60	−2.06	
HB	−1.29	−1.19	−1.50	
T	−1.20	−0.64	−0.95	
	Ti_8C_{12}	V_8C_{12}	Mo_8C_{12}	
HH	−0.04	−0.24	0.01	
HB	−1.09	−0.77	−0.93	
T	−1.31	−1.41	−1.73	

HH: M–C hybrid hollow site; HB: M–C hybrid bridge site; T: metal atop site. See the text for detail.

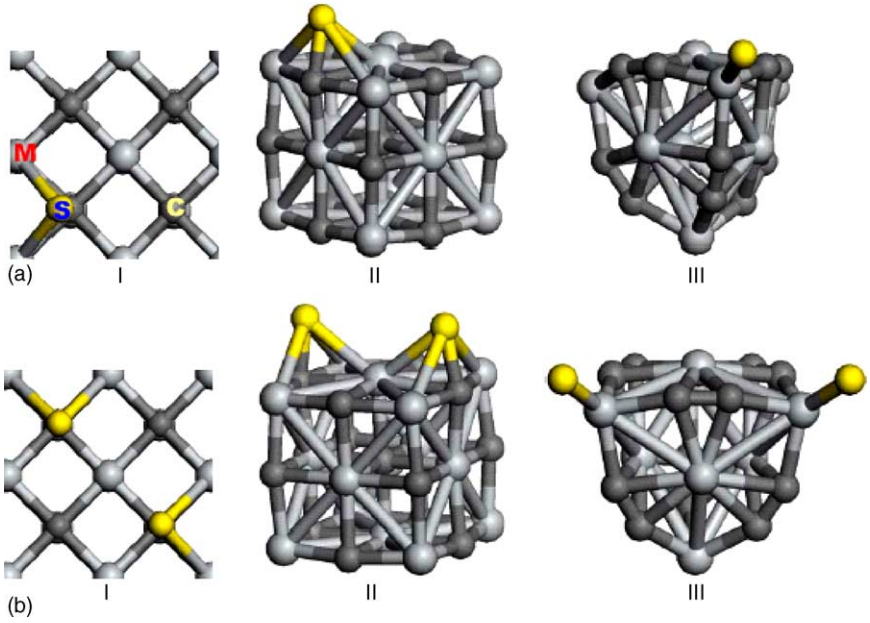

Fig. 2. The most stable configurations for the adsorption of S on the extended surfaces MC(0 0 1) ("HH", hybrid hollow site involving by two metal atoms and one carbon atom; upper: the top view; lower: the side view) (I), nanocrystals $M_{14}C_{13}$ ("HH", hybrid hollow site constructed by two M^o atoms, one M^i and one carbon atom) (II) and metcars M_8C_{12} ("T", M^o atop site) (III). (a) At a low coverage of S (1/4 ML for the surfaces) and (b) at a high coverage of sulfur (1/2 ML for the surfaces).

bonding with S and behave differently from the oxygen atoms of metal oxides which act as simple spectators in this process [52,53]. Such a phenomenon is commonly ignored [5,6,51] but it has been suggested by recent photoemission studies for the S/TiC(0 0 1) [13,31] and S/MoC_x systems [51].

Fig. 3a plots the energy of the strongest S adsorption at coverage of 1/4 ML on each carbide as a function of the C/M ratio. Here Mo_2C is also included as a reference. The C/M values of 0.5, 0.93, 1 and 1.5 correspond to Mo_2C, $M_{14}C_{13}$, MC and M_8C_{12}, respectively. In all the carbides, there is a charge transfer from the metal centers to the carbon centers (Fig. 4).

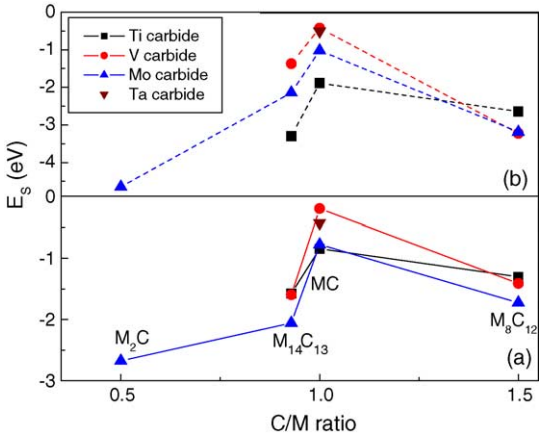

Fig. 3. Calculated S adsorption energies on the metal carbides at coverage of 1/4 ML (a) and 1/2 ML (b) as a function of the C/M ratio. The values shown in the figure correspond to the most stable configuration for S adsorption on each carbide as shown in Fig. 2. The C/M values of 0.5, 0.93, 1 and 1.5 correspond to Mo_2C, $M_{14}C_{13}$, MC and M_8C_{12}, respectively.

The DFT calculations have shown that Mo_2C(0 0 1) bonds to sulfur almost as strongly as pure Mo ($E_S = -2.68$ eV) (11). In contrast, the binding energies of S on MC(0 0 1) surfaces appear to be less than 2 eV (Fig. 3), as the positive charge on the metal centers increases (Fig. 4a). The weak bonding can be attributed to both ligand and ensemble effects [11,12,14,23]. As a result of the high C/M ratio, the electronic structure of the M atoms in the MC(0 0 1) surfaces changes (ligand effect) due to a substantial electron transfer from M to C (Fig. 4). For instance, the Mo atoms of a MoC(0 0 1) surface coordinated to five C atoms are more positively charged by ~0.5 e than those of Mo_2C(0 0 1) which have only one C neighbor (Fig. 4a). In general, the more positively charged

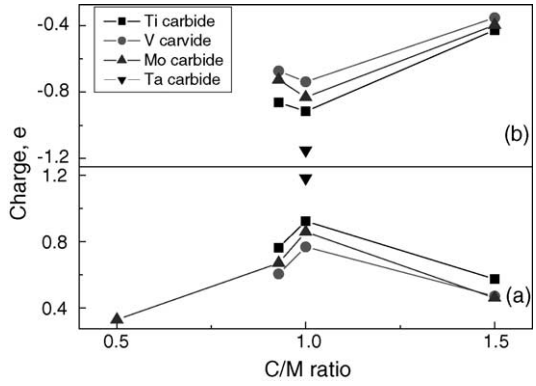

Fig. 4. Calculated charges of the exposed metal atoms (a) and carbon atoms (b) of the metal carbides as a function of the C/M ratio. The C/M values of 0.5, 0.93, 1 and 1.5 correspond to Mo_2C, $M_{14}C_{13}$, MC and M_8C_{12}, respectively. The charges of $M_{14}C_{13}$ and M_8C_{12} shown in (a) correspond to M^o. The charges of $M_{14}C_{13}$ and M_8C_{12} in (b) correspond to an average value.

the M atoms, the lower their d-band centers and therefore the lower their chemical activities [11,12,21,22]. In addition, increasing the C concentration also decreases the number of active M sites exposed in the surface (ensemble effect, Fig. 1) and thus the interaction between S and MC(0 0 1).

With a similar cubic structure and C/M ratio, the ensemble effect for the $M_{14}C_{13}$ nanocrystals is comparable to that of MC(0 0 1). The important difference comes from the existence of corner and edge sites in $M_{14}C_{13}$, which may exhibit high reactivity towards S [14,23]. For S adsorption on $M_{14}C_{13}$, M^o atop (T), M^o–M^i bridge (B), M^o–C hybrid bridge (HB) and hybrid hollow sites involving one C, one M^i and two M^o atoms (HH) (see Fig. 2b) were considered. The M^i atop site was not included since it has a low chemical reactivity as shown in our previous studies [14,23]. The bonding energies listed in Table 1 indicate that the HH site is the most stable configuration for S/$M_{14}C_{13}$. The M^o and C atoms of $M_{14}C_{13}$ interact very well with S. One can see that *the C atoms in the nanocrystals are actively involved in the bonding of S* as was seen for the MC(0 0 1) surfaces.

Although S adsorbed on both $M_{14}C_{13}$ and MC(0 0 1) prefers the HH sites, the adsorption on $M_{14}C_{13}$ is much stronger by 0.73–1.4 eV (Fig. 3). The M^o sites in the nanocrystal are less positively charged than the M sites of MC(0 0 1) (Fig. 4), and therefore have a higher activity (ligand effect). *These results illustrate the importance of corner and edge sites*. They will exist in steps and imperfections of a real MoC(0 0 1) surface, and provide extra reactivity with respect to the atoms in flat or ideal MoC(0 0 1) terraces.

M_8C_{12} adopts a different geometry and has a higher C/M ratio compared to $M_{14}C_{13}$ (Fig. 1b,c). However, the low-coordinated M^o atoms are also present in the metcars. M^o atop sites (T) (Fig. 2c), M^o–M^i bridge (B), hybrid M^o–C bridge sites (HB) and hybrid M^o–C–M^i hollow sites (HH) were studied for S adsorption on M_8C_{12}. According to the results in Fig. 3a, *the M_8C_{12} nanoparticles exhibit a much higher activity than the MC*(0 0 1) *surfaces by more than 0.5 eV in spite of the high C/M ratio*. Differently from MC(0 0 1) and $M_{14}C_{13}$, the metal T sites (I, Fig. 7a) rather than the high symmetric metal (B) and hybrid sites (HH and HB, see Table 1) are preferred in this case. To understand this, one has to consider ligand effects. As shown in Fig. 4a, the low-coordinated M^o atoms of M_8C_{12} are less positively charged than M^o sites of $M_{14}C_{13}$ or M sites of MC(0 0 1). It is important to notice in Table 1 that the M^o sites of M_8C_{12} are slightly less favorable than the HH sites of $M_{14}C_{13}$ (0.19–0.34 eV) for adsorbing sulfur. The C atoms of M_8C_{12} display a less negative charge than those of MC(0 0 1) and $M_{14}C_{13}$ (Fig. 4b). Thus, the C atoms interact directly with S in the cases of MC(0 0 1) and $M_{14}C_{13}$, while in M_8C_{12} the C atoms contribute only in an indirect way by donating a small amount of electrons through the M^o–S bonds.

Overall, our DFT results indicate that the C atoms may not be simple spectators in the chemisorption of sulfur on metal carbides. The reactivity of the metal carbides towards sulfur does not correlate with the C/M ratio. Comparing Figs. 3 and 4, one finds that the strength of the carbide-sulfur interactions correlates well with the charge of the exposed metal atoms. The less positively charged the metal atoms of the carbide, the stronger the interactions with S. These results highlight the importance of the ligand effects, with ensemble effects probably playing a secondary role. Ensemble effects could be important for the adsorption and dissociation of large S-containing molecules [12], but not for bonding of atomic sulfur.

In fact, our calculations also show that increasing the S exposure to 1/2 ML does not affect the preferential sites for S adsorption on each carbide (Figs. 5–7), except that in the case of Ti_8C_{12}, the Ti^o–C bridge site rather than the Ti^o atop site becomes more favorable at high coverage. In addition, the similar volcano variations of S adsorption energy with the C/M ratio are observed for both S coverages. In spite of the amount of S exposed, the activity of metal carbides towards S decreases following the sequence: $Mo_2C > M_{14}C_{13}, M_8C_{12} >$ MC (Fig. 3b). Mo_2C bonds S very strongly and therefore should be very reactive towards the reactions with atomic sulfur as product, such as thiophene or H_2S dissociation. Consequently, removing S becomes highly activated. In contrast, the S removal should be quite facile in the case of MC by displaying a weak S–MC interaction, while it is too inert to dissociate S-containing molecules. In fact, this phenomenon is also observed in the recent photoemission experiment, showing that Mo_2C is too reactive to remove S from the surface and MoC is too inert to adsorb and dissociate thiophene [54]. Therefore, following the Sabatier' principle, neither Mo_2C nor MC should be good HDS catalysts. It seems that $M_{14}C_{13}$ and M_8C_{12} may be good options by displaying a moderate chemical activity. Are the $M_{14}C_{13}$ and M_8C_{12} nanoparticles resistant to S ↔ C exchange and subsequent sulfidation?

3.3. Sulfidation of metal carbides

To avoid S-poisoning, the S chemisorbed onto several of the carbide systems must be removed by hydrogenation (i.e., H_2S formation) during the HDS processes. The formation of MoS_xC_y compounds eventually would lead to significant changes in the properties of the systems [5] and deactivation of the carbide catalysts [6,7,19]. In the present study, DFT was employed to calculate the energetics for the sulfidation of metal carbides through a S ↔ C exchange. The most stable configuration for S adsorption on each carbide was taken as the initial state (I, Figs. 5–7). The final state (F or F′) was constructed by S ↔ C site exchange (Figs. 5–7), where F is energetically favorable and the associated reaction energy is denoted as $\Delta E_1^{I,II}$ (I: coverage of 1/4 ML; II: coverage of 1/2 ML). In a previous work [55], it was found that the oxidation of the TiC(0 0 1) surface (O ↔ C exchange) was an exothermic process accompanied by the removal of C as CO and the formation of Ti oxides at large doses of O_2 above room temperature [55]. According to a recent study of S/TiC(0 0 1) [13], the S atoms were only chemisorbed on the surface even

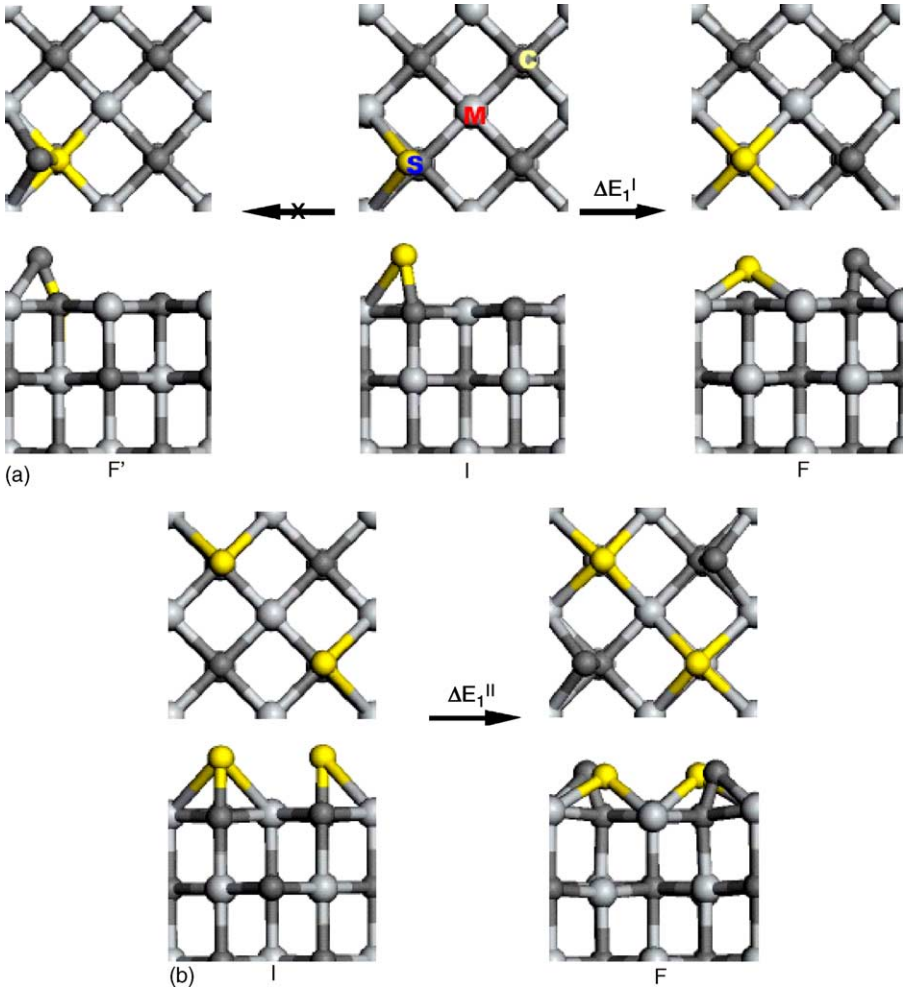

Fig. 5. Configurations of the initial (I) and final (F and F′) state for the sulfidation of the MC(0 0 1) surfaces (upper: the top view; lower: the side view). (a) At a low coverage of S (1/4 ML for the surfaces); (b) at a high coverage of sulfur (1/2 ML for the surfaces).

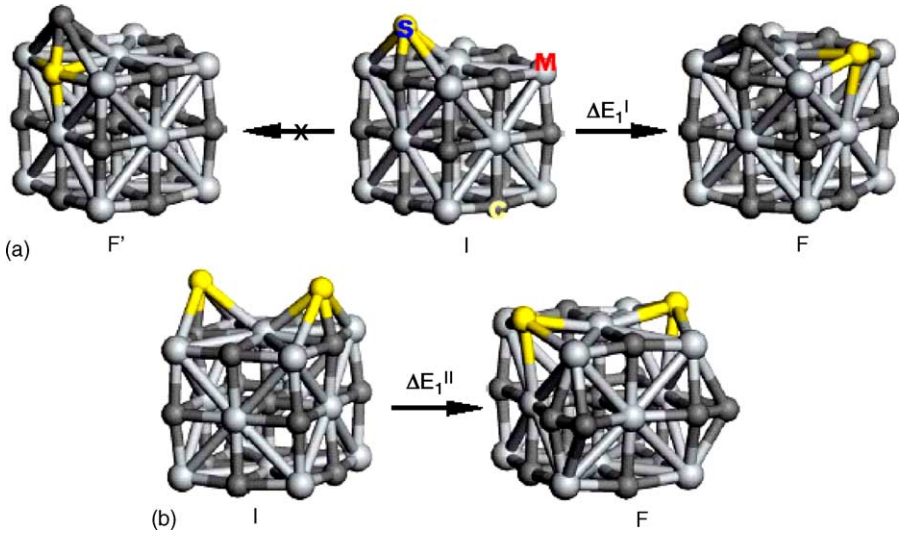

Fig. 6. Configurations of the initial (I) and final (F and F′) state for the sulfidation of the $M_{14}C_{13}$ nanoparticles. (a) At a low coverage of S (1/4 ML for the surfaces); (b) at a high coverage of sulfur (1/2 ML for the surfaces).

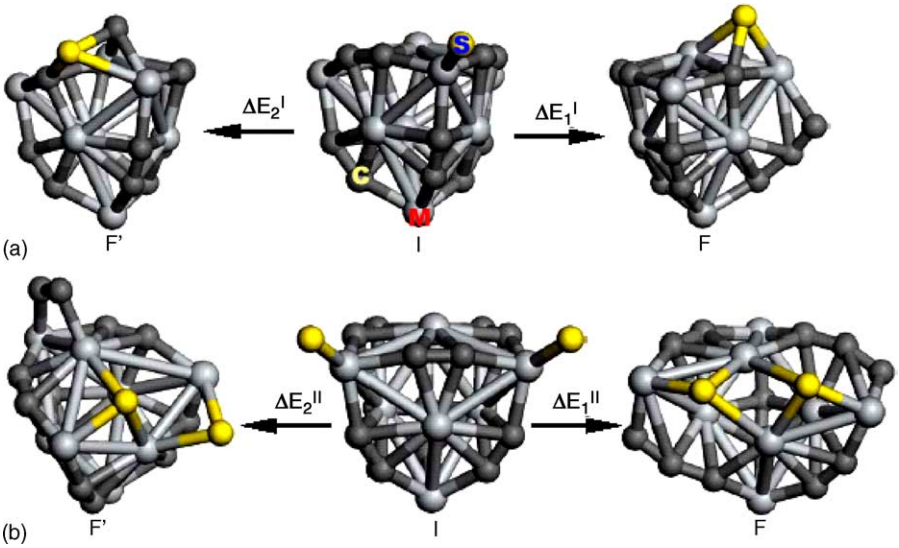

Fig. 7. Configurations of the initial (I) and final (F and F′) state for the sulfidation of the M_8C_{12} nanoparticles. (a) At a low coverage of S (1/4 ML for the surfaces); (b) at a high coverage of sulfur (1/2 ML for the surfaces).

at high temperature (550 K) and no formation of Ti sulfides was observed. The sulfidation of the other metal carbides has not been investigated at a fundamental level.

To compare with the experiments [13,55], we start with a TiC(0 0 1) surface. Our calculations show that at a S coverage of 1/4 ML, the conformation constructed by exchanging the positions of S and C of TiC(0 0 1) (F′, Fig. 5a) is not stable. Instead, the displaced C atoms spontaneously move to the nearby HH sites and form C–C bonds (F, Fig. 5a), a phenomenon also observed in the case of oxidation reactions [55]. However, even following the more favorable path I → F, the sulfidation of TiC(0 0 1) is still endothermic ($\Delta E_1^{\mathrm{I}} = 0.55$ eV). When the S coverage increases to 1/2 ML, $\Delta E_1^{\mathrm{I,II}}$ for 50% of the surface C atoms replaced by S (I → F, Fig. 5b) becomes as high as 3.64 eV. Thus, one can see that *the sulfidation of a flat TiC*(0 0 1) *surface is highly endothermic*. This is in accord with experimental observations [13]. Fig. 8 summarizes the energetics ($\Delta E_1^{\mathrm{I,II}}$) for the reaction I → F on the carbide surfaces (C/M = 1), indicating that *the sulfidation of VC*(0 0 1), *MoC*(0 0 1) *and TaC*(0 0 1) *is also endothermic* at a S coverage of 1/4 ML, and even more when increasing the coverage (1/2 ML) ($\Delta E_1^{\mathrm{II}} \gg \Delta E_1^{\mathrm{I}}$).

The simple exchange between the S atoms and the edge C atoms of $M_{14}C_{13}$ (F′, Fig. 6a) is also not stable. A spontaneous transformation from the S-embedded state to the initial S-adsorbed state was observed (F′ → I, Fig. 6a). Instead, a configuration with the S embedded at C sites and the displaced C atoms occupying nearby HH hollow sites is preferred (F, Fig. 6a). For this configuration, the sulfidation of the nanocrystals becomes exothermic ($\Delta E_1^{\mathrm{I}} = -1.03$ to -0.22 eV, Fig. 8). With increasing S coverage (Fig. 6b), the reaction energy increases a little ($\Delta E_1^{\mathrm{II}} = -0.47$ to 0.22 eV, Fig. 8), but it is still far lower than that of flat MC(0 0 1) surfaces under similar conditions by at least 3.2 eV. *The preferential sulfidation of $M_{14}C_{13}$ can be attributed to the presence of corner or edge sites*, as discussed in Section 3.2. Considering the structural similarities between the $M_{14}C_{13}$ nanocrystal and the step edges and kinks of the real MC(0 0 1) systems, one can expect that non-ideal MC(0 0 1) surfaces could undergo a sulfidation localized around defect sites. *The presence of these sites will be a necessary condition for the sulfidation of MC*(0 0 1).

The sulfidation of M_8C_{12} is much more difficult than that of $M_{14}C_{13}$. The ΔE_1's for the best options are displayed in Fig. 8, and they are in the range of 1–3.5 eV. Here, we ascribe the strong resistance of M_8C_{12} towards sulfidation to the high C/M ratio and the six C_2 groups. Comparing to

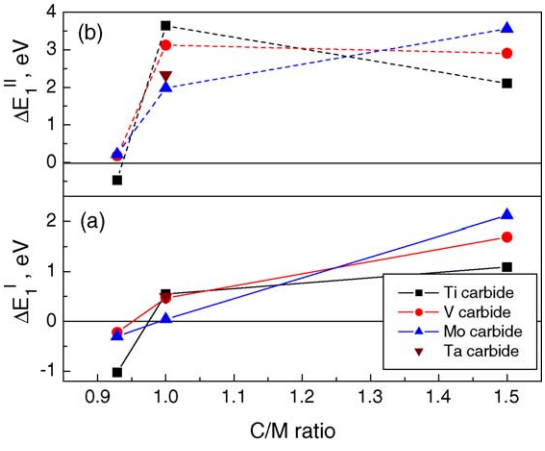

Fig. 8. Calculated reaction energies ($\Delta E_1^{\mathrm{I,II}}$) of the sulfidation on the metal carbides (I → F) as a function of C/M ratio. The C/M values of 0.5, 0.93, 1 and 1.5 correspond to Mo_2C, $M_{14}C_{13}$, MC and M_8C_{12}, respectively. (a) At a low coverage of S (1/4 ML for the surfaces); (b) at a high coverage of sulfur (1/2 ML for the surfaces).

the M^o–C–M^o bonds in nanocrystals, the favorable orbital overlap between the π-orbitals of the C_2 group and the d,s,p-orbitals of the metal sites gives rise to the bonding in M_8C_{12} (Fig. 4) [11,12,23].

Overall, in terms of S adsorption, Mo_2C and MC surfaces seem either too reactive or too inert to catalyze the HDS reactions, while both $M_{14}C_{13}$ and M_8C_{12} nanoparticles should be good catalysts by displaying a moderate activity in between Mo_2C and MC according to the Sabatier's principle. Considering the sulfidation (Fig. 8), on the other hand, the $M_{14}C_{13}$ nanocrystals are the most active. In contrast, both M_8C_{12} and flat MC(0 0 1) surfaces display a high resistance to the embedding of S atoms, and therefore the formation of MS_xC_y compounds. Among all these systems, the M_8C_{12} metcars appear as the best choice for a HDS catalyst. A recent DFT study based on a microkinetic model indicates that Ti_8C_{12} is able to catalyze the HDS of thiophene well [14], and the carbide should not be deactivated by the formation of TiS_xC_y compounds. We have found that the same is valid for Mo_8C_{12}.

4. Conclusion

DFT calculations were employed to investigate the sulfur adsorption and sulfidation of metal carbides, including extended surfaces MC(0 0 1) (M = Ti, V, Mo, Ta), $M_{14}C_{13}$ (M = Ti, V, Mo) nanocrystals and M_8C_{12} metcar (M = Ti, V, Mo) nanoparticles. Our results show that by raising the C/M ratio, the chemical activity of MC(0 0 1) towards S decreases substantially compared to Mo_2C, while $M_{14}C_{13}$ and M_8C_{12} nanoparticles exhibit a moderate chemical activity by including low-coordinated sites. The activity decreases following the sequence: $Mo_2C > M_{14}C_{13}, M_8C_{12} >$ MC. Flat MC(0 0 1) surfaces and M_8C_{12} nanoparticles display a high resistance to sulfidation. However, this process becomes much easier on $M_{14}C_{13}$ nanocrystals due to the presence of corner and edge sites in a cubic structure. Following Sabatier's principle, our calculations suggest that M_8C_{12} nanoparticles may display a catalytic performance better than the nanocrystals and bulk materials. The behavior of the M_8C_{12} systems is ascribed to their unique geometry. By introducing six pairs of C_2 groups, the M_8C_{12} system is stabilized, while the presence of the active M^o and M^i sites allows a moderate chemical activity.

Acknowledgements

This research was performed at Brookhaven National Laboratory under contract DE-AC02-98CH10886 with the US Department of Energy, Division of Chemical Sciences. The authors are also grateful to J.G. Chen for exchange of ideas on the catalytic behavior of metal carbides.

References

[1] A. Stanislaus, B.H. Cooper, Catal. Rev. Sci. Eng. 36 (1994) 75.
[2] C.N. Satterfield, Heterogeneous Catalysis in Industrial Practice, McGraw-Hill Inc., New York, 1991.
[3] P. Costa, J. Lemberton, C. Potvin, J. Manoli, G. Perot, M. Breysse, G. Djega-Mariadassou, Catal. Today 65 (2001) 195.
[4] H. Topsøe, B.S. Clausen, F.E. Massoth, Hydrotreating Catalysis, Springer-Verlag, Berlin, 1996.
[5] R.R. Chianelli, G. Berhault, Catal. Today 53 (1999) 357.
[6] D.J. Sajkowski, S.T. Oyama, Appl. Catal. A: Gen. 134 (1996) 339.
[7] P.A. Aegerter, W.W.C. Quigley, G.J. Simpson, D.D. Ziegler, J.W. Logan, K.R. McCrea, S. Glazier, M.E. Bussell, J. Catal. 164 (1996) 109.
[8] R.B. Levy, M. Boudart, Science 181 (1973) 547.
[9] J.G. Chen, Chem. Rev. 96 (1996) 1447;
H.H. Hwu, J.G. Chen, Chem. Rev. 105 (2005) 185.
[10] J. Chen, J. Eng, S.P. Kelty, Catal. Today 43 (1998) 137.
[11] P. Liu, J.A. Rodriguez, J. Chem. Phys. 120 (2004) 5414;
P. Liu, J.A. Rodriguez, J. Chem. Phys. 119 (2004) 10895.
[12] P. Liu, J.A. Rodriguez, J.T. Muckerman, J. Phys. Chem. B 108 (2004) 15662;
P. Liu, J.A. Rodriguez, J.T. Muckerman, J. Chem. Phys. 121 (2004) 10321.
[13] J.A. Rodriguez, P. Liu, J. Dvorak, T. Jirsak, J. Gomes, Y. Takahashi, K. Nakamura, Phys. Rev. B 69 (2004) 115414.
[14] P. Liu, J.A. Rodriguez, J.T. Muckerman, J. Phys. Chem. B 108 (2004) 18796.
[15] P. Sabatier, Ber. Deutsche Gem. Ges. 44 (1911) 2001;
M. Boudart, G. Djèga-Mariadassou, Kinetics of Heterogeneous Catalytic Reactions, Princeton University Press, New York, 1984.
[16] T.P. St. Clair, S.T. Oyama, D.F. Cox, Surf. Sci. 511 (2002) 294.
[17] B. Dhandapani, T. St. Clair, S.T. Oyama, Appl. Catal. A: Gen. 168 (1998) 219.
[18] T. Xiao, H. Wang, A.P.E. York, M.L.H. Green, Catal. Lett. 83 (2002) 241.
[19] B. Diaz, S.J. Sawhill, D.H. Bale, R. Main, D.C. Phillips, S. Korlann, R. Self, M.E. Bussell, Catal. Today 86 (2003) 191.
[20] M. Neurock, J. Catal. 216 (2003) 73.
[21] J. Greeley, J.K. Nørskov, M. Mavrikakis, Annu. Rev. Phys. Chem. 53 (2002) 319.
[22] B. Hammer, J.K. Nørskov, Chemisorption and Reactivity on Supported Clusters and Thin Films, Kluwer Academic Publishes, Netherlands, 1997.
[23] P. Liu, J.A. Rodriguez, H. Hou, J.T. Muckerman, J. Chem. Phys. 118 (2003) 7737.
[24] H. Hou, J.T. Muckerman, P. Liu, J.A. Rodriguez, J. Phys. Chem. A 107 (2003) 9344.
[25] G. von Helden, A.G.G.M. Tielens, D. van Heijnsbergen, M.A. Duncan, S. Hony, L.B.F.M. Waters, G. Meijer, Science 288 (2000) 313;
G. von Helden, D. van Heijnsbergen, M.A. Duncan, G. Meijer, Chem. Phys. Lett. 333 (2001) 350.
[26] M.M. Rohmer, M. Benard, J.M. Poblet, Chem. Rev. 100 (2000) 495.
[27] B.D. Leskiw, A.W. Castleman, C. R. Physique 3 (2002) 251.
[28] B. Delley, J. Chem. Phys. 92 (1990) 508;
B. Delley, J. Chem. Phys. 113 (2000) 7756.
[29] M. Miletic, J.L. Gland, K.C. Hass, W.F. Schneider, J. Phys. Chem. B 107 (2003) 157.
[30] A. Maiti, J.A. Rodriguez, M. Law, P. Kung, J.R. McKinney, P. Yang, Nano Lett. 3 (2003) 1025.
[31] J.A. Rodriguez, P. Liu, J. Dvorak, T. Jirsak, J. Gomes, Y. Takahashi, K. Nakamura, Surf. Sci. 543 (2003) 675.
[32] B. Hammer, L.B. Hansen, J.K. Nørskov, Phys. Rev. B 59 (1999) 7413.
[33] G.K. Gueorguiev, J.M. Pacheco, Phys. Rev. B 68 (2003) 241401;
G.K. Gueorguiev, J.M. Pacheco, Phys. Rev. Lett. 88 (2002) 115504.

[34] D. van Heijnsbergen, G. von Helden, M.A. Duncan, A.J.A. van Roij, G. Meijer, Phys. Rev. Lett. 83 (1999) 4983.
[35] J.S. Pilgrim, M.A. Duncan, J. Am. Chem. Soc. 115 (1993) 6958.
[36] M.A. Duncan, J. Cluster Sci. 8 (1997) 239.
[37] J.A. Rodriguez, J.M. Ricart, A. Clotet, F. Illas, J. Chem. Phys. 115 (2001) 454.
[38] Z. Yang, R. Wu, J.A. Rodriguez, Phys. Rev. B 65 (2002) 155409.
[39] R.S. Mulliken, J. Chem. Phys. 23 (1955) 1833.
[40] K.B. Wiberg, P.R. Rablen, J. Comput. Chem. 14 (1993) 1504.
[41] H. Chang, J.F. Harrison, T.A. Kaplan, S.D. Mahanti, Phys. Rev. B 49 (1994) 15753.
[42] C.W. Bauschlicher Jr., P.S. Bagus, J. Chem. Phys. 81 (1984) 5889.
[43] A. Dunand, H.D. Flack, K. Yvon, Phys. Rev. B 31 (1985) 2299.
[44] S.V. Didziulis, P. Frantz, L.C. Fernandez-Torres, R.L. Guenard, O. El-bjeirami, S.S. Perry, J. Phys. Chem. B 105 (2001) 5196.
[45] H.W. Hugosson, L. Nordström, U. Jansson, B. Johansson, O. Eriksson, Phys. Rev. B 60 (1999) 15123.
[46] L.I. Johansson, Surf. Sci. Rep. 21 (1995) 177.
[47] F. Vies, C. Sousa, P. Liu, J.A. Rodriguez, F. Illas, J. Chem. Phys. 122 (2005) 174709.
[48] J.A. Rodriguez, J. Hrbek, J. Acc. Chem. Res. 32 (1999) 719.
[49] J.A. Rodriguez, J. Dvorak, T. Jirsak, G. Liu, J. Hrbek, Y. Aray, C. Gonzalez, J. Am. Chem. Soc. 125 (2003) 276.
[50] J. Gottschalck, B. Hammer, J. Chem. Phys. 784 (2002) 116.
[51] J.A. Rodriguez, J. Dvorak, T. Jirsak, J. Phys. Chem. B 104 (2000) 11515.
[52] E.L.D. Hebenstreit, W. Hebenstreit, U. Diebold, Surf. Sci. 470 (2001) 347.
[53] J.A. Rodriguez, J. Hrbek, Z. Chang, J. Dvorak, T. Jirsak, A. Maiti, Phys. Rev. B 65 (2002) 235414.
[54] P. Liu, J.A. Rodriguez, T. Asakura, J. Gomes, K. Nakamura, J. Phys. Chem. B 109 (2005) 4575.
[55] J.A. Rodriguez, P. Liu, J. Dvorak, T. Jirsak, J. Gomes, Y. Takahashi, K. Nakamura, J. Chem. Phys. 121 (2004) 465.